

Supporting Information

SI Materials and Methods

Animals. C75BL/6J, C3H/HeJ and nude mice were used in this study. K14-GFP, Pdgfra-EGFP, Sox2-EGFP, and FVB-GFP mice lines were purchased from Jackson laboratory. K14-GFP/Lef1-RFP mouse were kindly gifted from Dr. Elaine Fuchs laboratory. All procedures were performed upon approval of USC IACUC.

Alkaline Phosphatase Staining. Cell cultures were washed twice with PBS, fixed with 4% paraformaldehyde (PFA) at 4°C for 1h, and developed with BCIP (5-bromo-4-chloro-3-indolyl-phosphate) in conjunction with NBT (nitro blue tetrazolium, Bio-Rad, Richmond, CA) in the dark at room temperature for 10 min. After washing with PBS, the stained samples were imaged under a phase-contrast microscope.

Hematoxylin and eosin (H&E) staining, Immunofluorescence, and in Situ Hybridization

Cell cultures for H&E staining, immunofluorescence staining, in situ hybridization and TUNEL staining were fixed in DEPC-treated 4% PFA buffer at 4°C overnight. Paraffin-embedded tissue was cut into 8µm sections.

For H&E staining, the sections were incubated with hematoxylin and eosin for 2 min, respectively at room temperature, dehydrated with ethanol and mounted with resinene.

For immunofluorescence staining, the samples were dewaxed and rehydrated, and retrieved with 10 mM sodium citrate buffer (pH 6.0) at 100°C for 10 min. Then the samples were blocked with 1% bovine serum albumin (BSA) buffer for 1h, incubated with primary antibodies (Table S2) at 4°C overnight and secondary antibodies conjugated with Alexa 488 or 594, respectively (1:1000, Life

Technologies) at 37 °C for 2 h. Samples were washed, counterstained with propidium iodide (PI) or 4'6'-diamidino-2-phenylindole (DAPI) and mounted with glycerol. Images were taken under a LSM 510 meta confocal microscope (USC Center for Liver Diseases).

For in situ hybridization, the sections were dewaxed and rehydrated, incubated with 1.5ug/ml proteinase K in PBT at 37°C for 20 min, then washed with PBT, acetylated with 0.25% acetic anhydride / triethanolamine, dehydrated with a graded ethanol series. The slides were put into a moisture chamber, added with 200ul hybridization solution, covered with a plastic coverslip and incubated at 65°C overnight. After washing with SSC and MBST buffer, the samples were incubated with Anti-Dig-AP conjugated antibody at 4°C overnight, washed with NTMT, developed with NBT/BCIP (Roche) buffer, counterstained with eosin and mounted with resinene. The sequences of oligonucleotides used for probe production are listed in Table S3.

TUNEL Staining. Paraffin-embedded tissue was cut into 8um sections. “*In situ* Keratinocyte Death Detection Kit” (Roche Diagnostics, Basel, Switzerland) was used for TUNEL staining(1). After dewaxing and rehydration, the sections were incubated with 20ug/ml proteinase K in 10mM Tris 7.5 and 5 mM EDTA for 15 min at room temperature. Then the sections were rinsed with PBS and 50ul TUNEL reaction cocktail was added. They were then incubated in a humidified chamber for 1 hour at 37°C in the dark. The samples were then counterstained with PI and mounted with glycerol.

Small Molecules Perturbation and Recombinant Protein Treatment. Libraries of small molecule inhibitors were a gift from Dr. Qing Liu and Dr. Justin Ichida at the USC CIRM Center. Small molecules or recombinant proteins at different concentrations were added into the culture medium. For live-imaging study, small molecules are added 3 hours before filming. Names, catalog number and concentrations of small molecules are listed in Table S4. After treatment with small molecules or

recombinant proteins, the samples were cut into sections at 8 μ m, and stained with K14 or other antibodies to visualize phenotypic alterations, such as changes in aggregate size, coalescence and planarization. Aggregate cell numbers were counted using Imaris software. Length of the differentiated aggregate region was measured with a ruler in Adobe Photoshop CS3. The aggregate coalescence rate was counted in 20 whole-mount images at 10X magnification.

RNA-seq Preparation and Sequencing. RNA-seq was performed on replicate samples from different culture time points. For all samples, RNA was extracted using TRIzol reagent (Invitrogen) from combined epidermal and dermal cells. 5 μ g total RNA from each sample was used to prepare the RNA-seq libraries using TruSeq RNA sample preparation v2 kit (Illumina). The libraries were sequenced by Hi-seq 2000 at the University of Southern California Epigenome Center. RNA-seq raw data were accessible at NCBI GEO (accession number: GSE86955).

Transcriptome Analyses. The mouse mm9 reference genome, and RefSeq genome annotation downloaded from the UCSC Genome Browser were used for RNA-Seq analysis(2). The alignment, quantification, normalization, and differentially expression analysis were performed by STAR 2.4.1d (3), HTSeq-count 0.6.0 (4), TMM (5), and edgeR 3.10.5 (6), respectively. False discovery rate < 0.05 was set as a threshold to identify differentially expressed genes. The principal component analysis (PCA), hierarchical clustering, and Venn diagrams were carried out by Partek Genomics Suite 6.15.1207 (Partek Inc.). DAVID 6.7 was run for gene set enrichment analysis (7). The top enriched pathways from “Gene ontology” and “Pathways” with the significant p-value ($p < 0.05$) were presented in Table S1. Genes with detectable RPKM (Reads Per Kilobases per Million reads) value (usually larger than 25) were selected to do further expression study. We chose some of genes involved in the top enriched pathways that have differential expression between different time points to do functional study. In addition, the phenotypes observed in the morphological transition processes were also

matched with functional annotations, to target the potential genes or pathways in these highly enriched pathways for further studies.

Transplantation. Cell cultures from different culture conditions or treatments (Fig. 1, 6 and SI Appendix, Fig. S2, 7 and 8) were transplanted onto the dorsum of nude mice to test the hair forming efficiency according to our previously developed planar hair forming assay (8). For the reconstitution assay, we found there is no significant difference of the self-organization process if we use different numbers of newborn mouse cells in a droplet. Because of harder availability of adult cells, we used different numbers of cells from adult and newborn mice for doing reconstitution assay. Usually we use 5×10^6 epidermal cells and 4.5×10^7 dermal cells in one droplet for newborn cell culture. We use 2×10^6 epidermal cells and 1.8×10^7 dermal cells for adult cell culture. After transplantation, five 1mm^2 areas with regenerated hair follicles were counted and then averaged. Total regenerative area was measured. In our experience, the regenerative area is about 0.5 cm^2 from newborn cell culture grafts, and 0.2 cm^2 from adult cell culture grafts. Nine replicates were used.

Cell sorting. Dorsal skins from neonatal K14-H2BGFP and Pdgfra-EGFP mice were dissected and treated overnight with 0.025% trypsin (Gibco) at 4°C , which separated the epidermis and dermis. The epidermis and dermis were further dissociated into single cells by treatment with 0.25% trypsin or 0.35% collagenase, respectively, for 30 min at 37°C . Then the epidermal cells from K14-H2BGFP and dermal cells from Pdgfra-EGFP mice were incubated with DAPI to exclude dead cells. Cell isolations were performed on cell sorters at the USC Flow Cytometry Core Facility. The isolated K14-GFP positive epidermal cells and Pdgfra-EGFP dermal cells were mixed in a ratio of 1:9 and cultured accordingly.

Statistical analyses. All experiments were repeated at least four times and the results were expressed as mean \pm SD. Statistical significance among experimental and control groups were evaluated using the Student's t test. A value of $p < 0.05$ was considered as statistically significant. Errors in the raw cluster frequency counts were estimated as 10% based on the counting accuracy at which the data were collected. The errors in the cluster size distributions (Figs. 2F and S2G) were then calculated using standard error propagation, assuming independent errors in different size bins.

Cell tracking analysis. Epidermal cells were tracked using Imaris software, using the “Brownian” movement model, with a maximum displacement between frames of $20\mu\text{m}$. Tracked movies were visually inspected for tracking accuracy. The median velocity of all cells was removed for each frame to correct for drift.

We calculated the directional autocorrelation to see how quickly cells stray from their direction of movement (Fig. 2E). For comparison we also calculated the expected directional correlation (as if cells are choosing the angle of movement at in each frame randomly) from 10^6 randomly sampled angles in the intervals of $\pm\pi/4$, $\pm\pi/2$, and $\pm3\pi/4$. Due to the fact the interframe interval of the video microscopy data varies slightly between data sets (due to different image stack heights), the lag for the correlation also varied. To visualize the data across multiple experiments, we therefore calculated the directional autocorrelation for each data set, then fitted a smooth surface over the scattered pooled data using bicubic interpolation (using the Matlab file exchange function RegularizeData3D with smoothness parameter 10^{-4}).

Mathematical modelling. The Smoluchowski coagulation equations (9) describe the change in the distribution of irreversibly aggregating particles in space and time. We restrict ourselves to the well-mixed case, where the number, n_s , of clusters of size s evolves according to:

$$\frac{dn_s(t)}{dt} = \frac{1}{2} \sum_{i=1}^{s-1} K_{i,s-i} n_i(t) n_{s-i}(t) - \sum_{i=1}^{\infty} K_{s,i} n_s(t) n_i(t)$$

Here, $K_{i,j}$ is the kinetic kernel (or coagulation kernel) that gives the rate at which clusters of size i and j aggregate. This rate is proportional to the size and motility of the aggregates (Fig. S3F).

To fit the above equation to data, we used monodisperse (dissociated single-cells) initial conditions. To numerically approximate solution of the equations for infinite cluster sizes, we checked convergence of the numerical solutions for cluster sizes of up to 400 cells (the range spanned by the data) by including additional (unobserved) cluster sizes in our equations until convergence was satisfactory.

Scaling analysis. We investigated whether clustering epidermal cells have the same scaling behavior as the hypothesized aggregation process, and thus whether they belong to the universality class of “clustering of clusters” (10, 11). In this process, diffusing (or otherwise moving) particles merge into particles of larger size upon contact, and these larger particles continue to move and merge upon contact with further particles. This class of models exhibits scale invariance, meaning that we should be able to describe the dynamics fully (at a coarse level) by the change in the average cluster size over time. To rescale the cluster size distribution, we divided the cluster size by the mean cluster size at a given time (Fig. S3G). When rescaling the argument of the distribution function in this way, we need to multiply by the average cluster size to conserve overall probability normalization.

Supplementary References

1. Lei M, *et al.* (2012) Gsdma3 is a new factor needed for TNF-alpha-mediated apoptosis signal pathway in mouse skin keratinocytes. *Histochem Cell Biol* 138(3):385-396.
2. Rosenbloom KR, *et al.* (2015) The UCSC Genome Browser database: 2015 update. *Nucleic Acids Res* 43(Database issue):D670-681.
3. Dobin A, *et al.* (2013) STAR: ultrafast universal RNA-seq aligner. *Bioinformatics* 29(1):15-21.
4. Anders S, Pyl PT, & Huber W (2015) HTSeq--a Python framework to work with high-throughput sequencing data. *Bioinformatics* 31(2):166-169.

5. Robinson MD & Oshlack A (2010) A scaling normalization method for differential expression analysis of RNA-seq data. *Genome Biol* 11(3):R25.
6. Robinson MD & Smyth GK (2008) Small-sample estimation of negative binomial dispersion, with applications to SAGE data. *Biostatistics* 9(2):321-332.
7. Huang da W, Sherman BT, & Lempicki RA (2009) Systematic and integrative analysis of large gene lists using DAVID bioinformatics resources. *Nat Protoc* 4(1):44-57.
8. Lee LF, Jiang TX, Garner W, & Chuong CM (2011) A simplified procedure to reconstitute hair-producing skin. *Tissue Eng Part C Methods* 17(4):391-400.
9. Von Smoluchowski M (1916) Three discourses on diffusion, Brownian movements, and the coagulation of colloid particles. *Physikalische Zeitschrift der Sowjetunion* 17 557-571.
10. Botet R & Jullien R (1984) Size distribution of clusters in irreversible kinetic aggregation. *Journal of Physics A: Mathematical and General* 17(12):14.
11. Kolb M (1984) Unified Description of Static and Dynamic Scaling for Kinetic Cluster Formation. *Physical review letters* 53(17):4.

Supplementary figures and legends

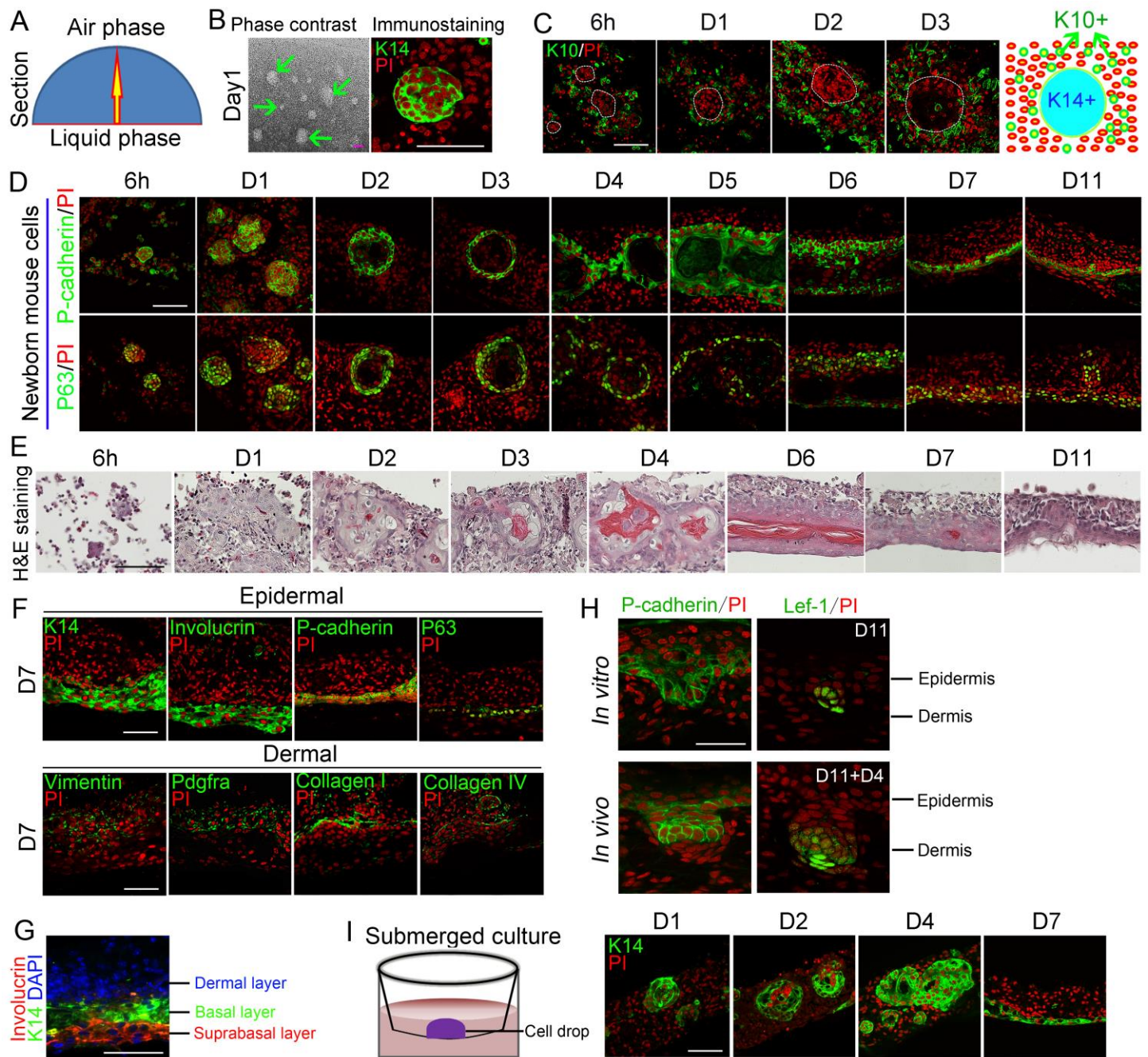


Fig. S1. The process of self-organization from dissociated cells to planar skin with hair placode-like structure formation. (A) All sections in the present study are cut in side view. (B) Phase-contrast microscope image shows white patches representing aggregates at day 1. Immunostaining shows all the cells in the aggregates are K14 positive, indicating they originated from basal epidermal cells. (C) K10+ suprabasal epidermal cells are not involved in aggregate formation. (D) Immunostaining for P-cadherin and P63 shows the stepwise self-organization processes of epidermal cells. (E) H&E

staining shows more time points of the skin progenitor cell self-organization process. (F) Markers for epidermal and dermal cells reveal formation of skin with epidermal and dermal components at day 7. (G) Immunostaining for Involucrin and K14 shows stratification of epidermis at day 10 in culture. (H) P-cadherin and Lef-1 immunostaining show hair placode and dermal condensation formation during skin reconstitution *in vitro* and *in vivo*. D11+ D4 represents cells are cultured for 11 days *in vitro* and 4 days after transplantation. (I) Self-organization of skin cells in submerged culture condition. Scale bars=50um, 100um.

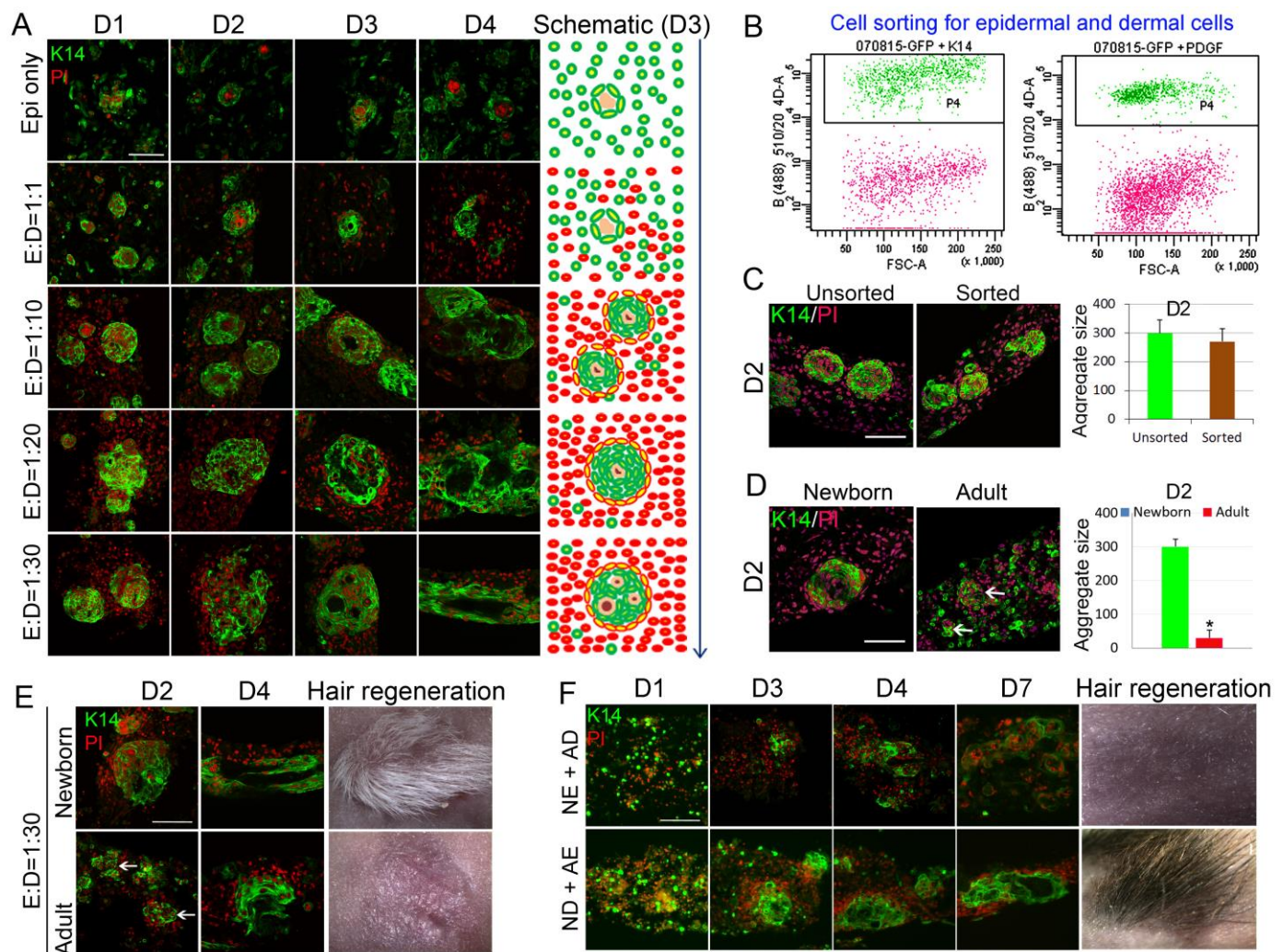


Fig. S2. (A) K14 immunostaining reveals higher ratios of epidermal: dermal cells result in smaller aggregate formation. (B) FACS sorting of epidermal and dermal cells using K14-GFP and Pdgfra-EGFP mouse lines, respectively. (C) Culture of FACS-sorted epidermal and dermal cells form smaller

aggregates at day 2, when compared to the control. (D) Immunostaining for K14 shows only small aggregates form when culturing cells from adult mice using the same method. (E) Adult cells that are cultured at 1:30 E:D ratio form larger aggregates when compared to those cultured at 1:9 E:D ratio (D) at day 2. The epidermal cells undergo terminal differentiation and fail to coalesce at day 4. The aggregates are smaller in size when compared to the newborn mouse cultures at 1:30 E:D ratio. The adult cells fail to regenerate hairs upon transplantation to the nude mice. (F) Recombination assay of newborn and adult cells. A, adult cells. N, newborn cells. Epi, E, epidermal cells. D, dermal cells. Scale bars=100um. Data are reported as average \pm SD, *p < 0.05. n>100.

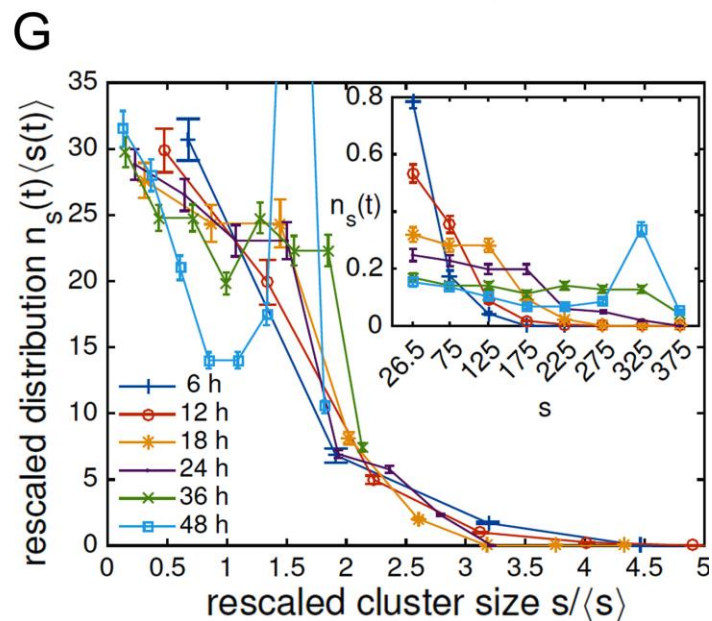
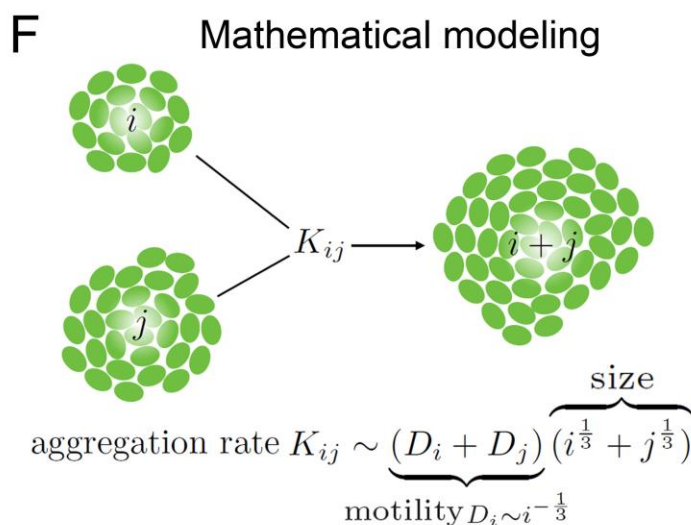
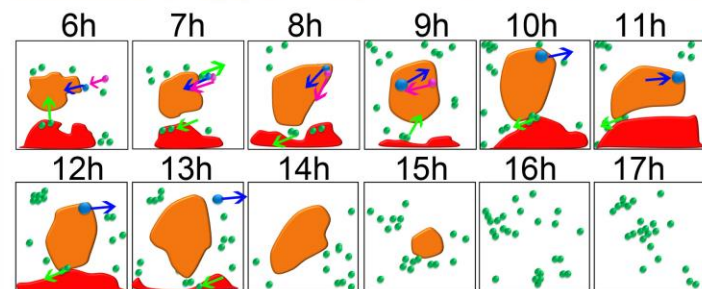
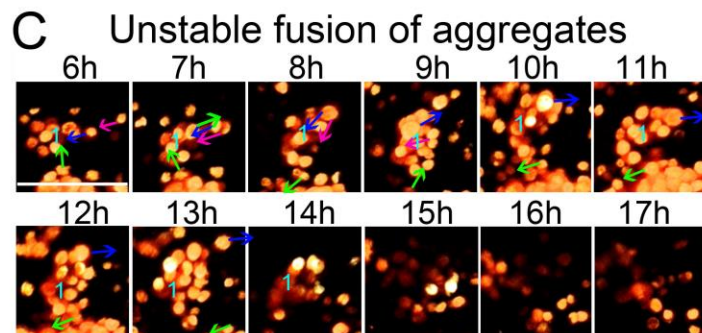
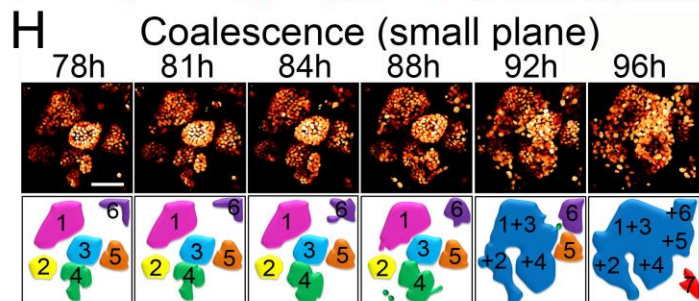
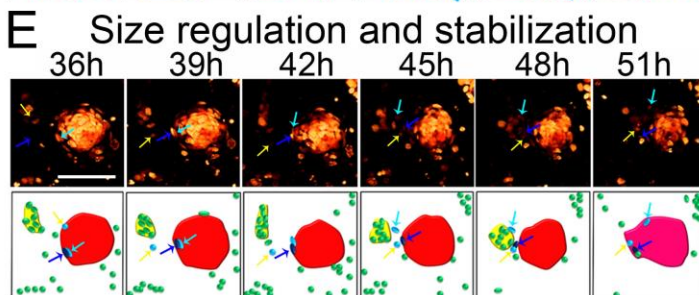
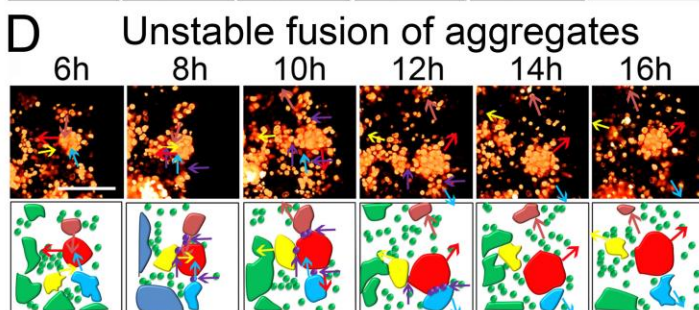
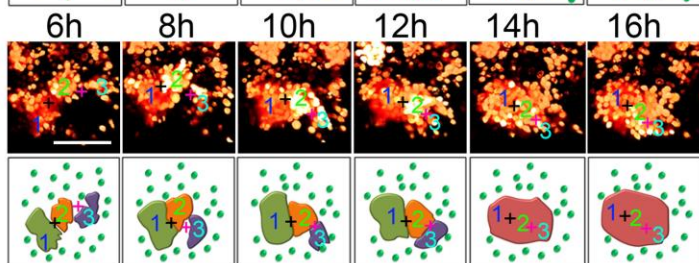
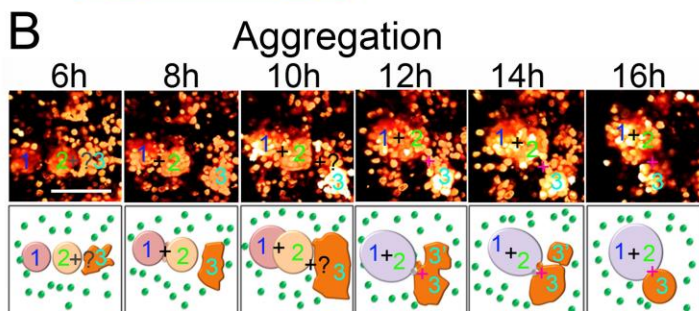
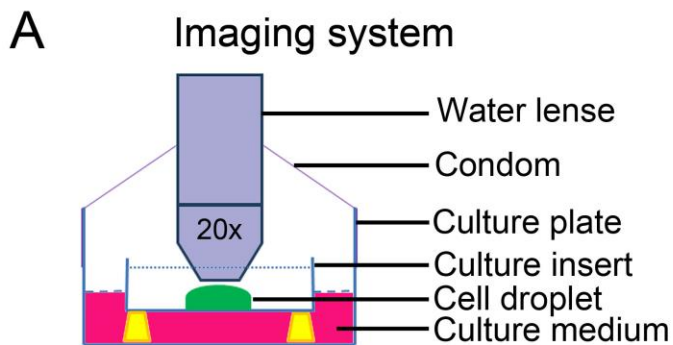


Fig. S3. Time lapse live-imaging shows cell behaviors of epidermal cells using a K14-GFP transgenic mouse line. (A) Time lapse live-imaging system setup. Condom membrane is used to prevent culture medium evaporation. (B) Aggregates merging. Scale bar, 100um. (C) Individual cells can enter and leave the aggregates. Scale bar, 100um. (D) Aggregates can form and disaggregate. Scale bar, 100um. (E) Cells can leave one aggregate and enter another aggregate, and then merge back to the original one. Scale bar, 100um. (F) Illustration of aggregation model. Epidermal clusters of size i and j aggregate with rate K_{ij} , which in turn depends on the cluster motility and size. (G) Epidermal cell cluster size distributions from the first 36 hours collapsed onto each other when rescaled by the average cluster size for each time-point, showing statistical self-similarity. Lack of collapse for the 48h curve indicates a change in the cluster growth dynamics. The unscaled data show no collapse (inset). (H) Aggregates that have close distance can merge together from day 3.5 to day 4. Scale bars=100um. $n \geq 500$.

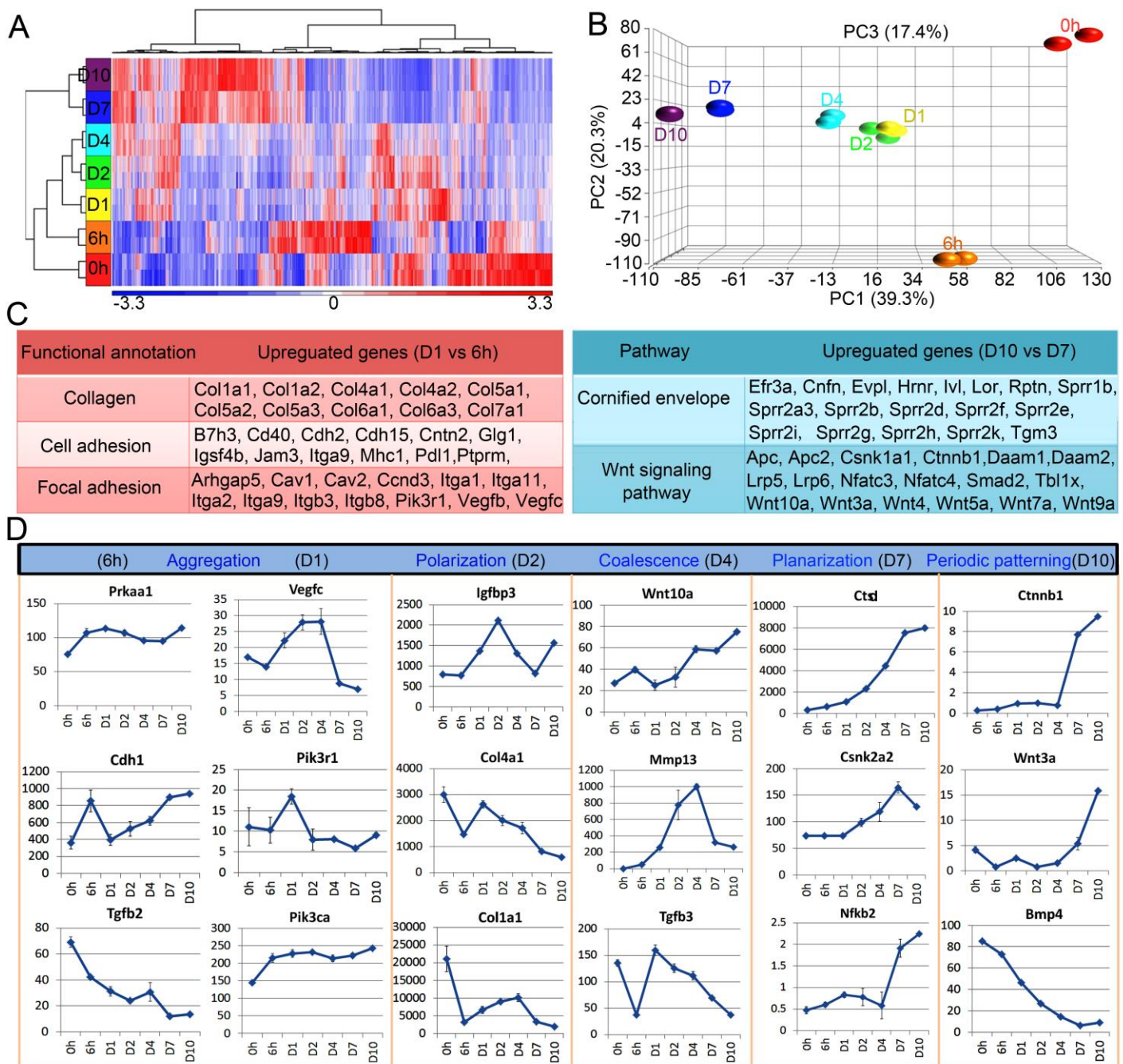


Fig. S4. RNA-seq profiling and bio-informatic analysis reveal key molecular events during self-organization process. (A) Hierarchical clustering shows genes that are dynamically expressed at different time points. (B) Principal component analysis (PCA) shows replicates cluster together. (C) Functional annotations show pathways and genes that are increased at different time points. (D) Exemplary genes that are dynamically expressed at different time points.

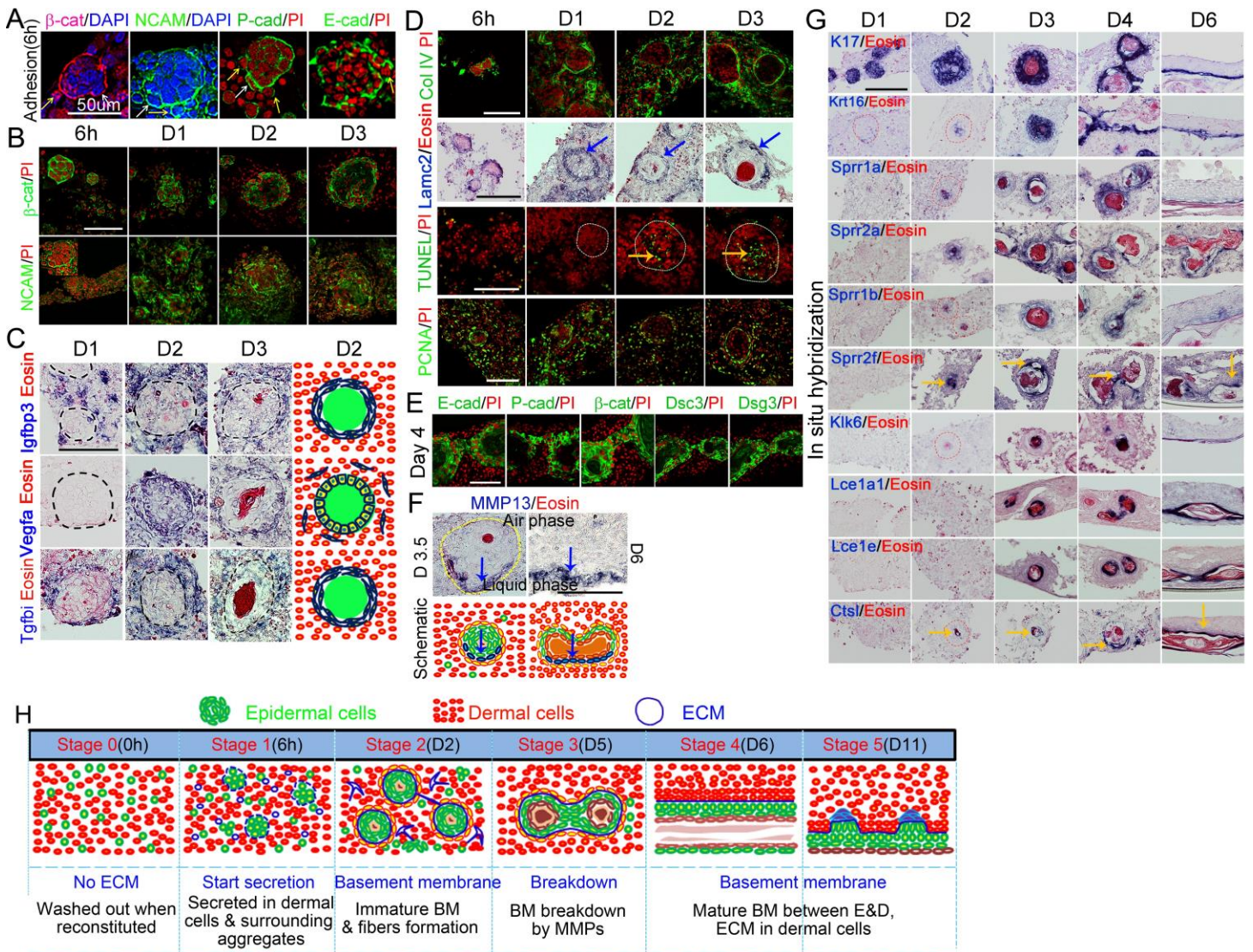


Fig. S5. Immunostaining and in situ show gene expression at different phases. (A). Immunostaining shows adhesion molecules including b-catenin, NCAM, P-cadherin and E-cadherin are highly expressed at 6h. (B) Immunostaining shows adhesion genes including b-catenin is expressed in epidermal aggregates, and Ncam is expressed higher in epidermal aggregates and lower in the dermal cell region. (C) In situ shows mRNA expression of different genes. IGFBP3 is expressed in the dermal cell region and becomes more intense surrounding the aggregates at day 2 and day 3. Vegfa appears in the dermal cell region and basal layer of the epidermal aggregate from day 2. Tgfbi is always expressed in the dermal cells surrounding the aggregates. (D) Immunostaining shows collagen type IV is expressed at the dermal region and form a basement membrane at day 2, which gets more mature at day 3. In situ hybridization shows Lamc2 is expressed at the border of the

aggregate, forming the basal layer. TUNEL staining shows more cell apoptosis in the center of the aggregate from day 2. PCNA staining shows cell proliferation in the outer part of the aggregates from day 2. (E) Immunostaining for epidermal cell markers shows an epidermal cell chain links two aggregates. (F) In situ hybridizations show *Mmp13* is preferentially expressed at the lower part of aggregates at day 3.5 day 6. (G) In situ shows mRNA expression of epidermal cell differentiation genes at different time points. (H) Schematic drawing shows ECM assembly during skin cell self-organization. Scale bars= 100um. n=9.

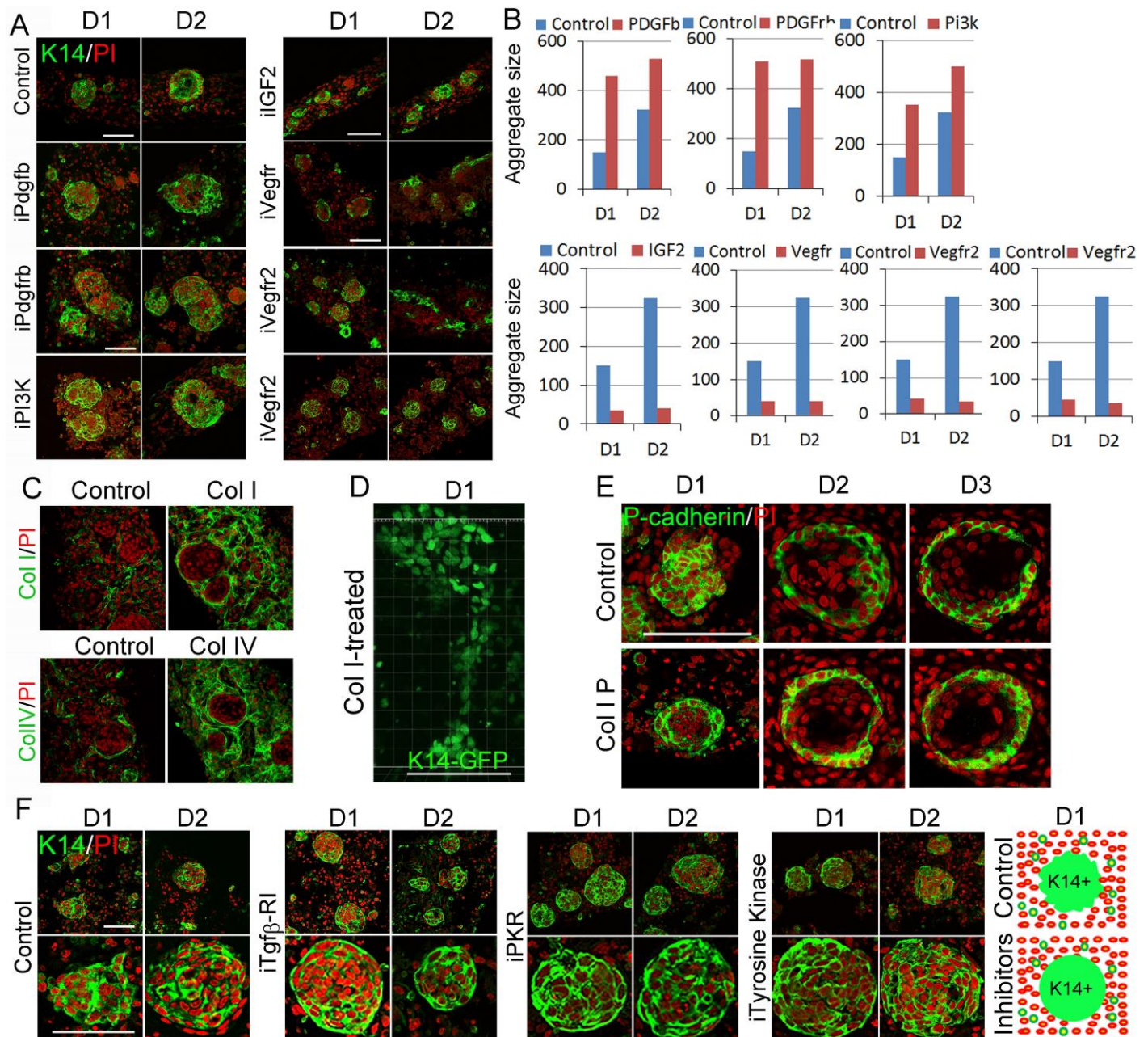


Fig. S6. Molecular mechanisms of the self-organization process from dissociated cells to polarized aggregates. (A) Immunostaining for K14 shows epidermal aggregates can grow larger when treated with small molecules that inhibit Pdgfb, Pdgfrb and PIK3, or grow smaller when treated with small molecules that inhibit IGF2 Vegfr, and Vegfr2. (B) Statistical analysis show the size of aggregates after the cultures are treated by small molecules inhibitors at day 1 and day 2. (C) Immunostaining shows expression of Collagen I and Collagen IV is increased after the cultures were treated by Collagen I and Collagen IV recombinant proteins. (D). Live-imaging analysis reveals long epidermal strand formation at day 1 after the culture was treated by Collagen I recombinant protein. Scale bar, 100um. (E). Immunostaining for P-cadherin shows over expressed Col I leads to premature polarization of the aggregates. (F). Smooth boarded aggregate formation at day 1 after the cultures were treated by small molecules that inhibit Tgfb-RI, PKR and Class III tyrosine Kinase. Scale bar, 100um. n=9.

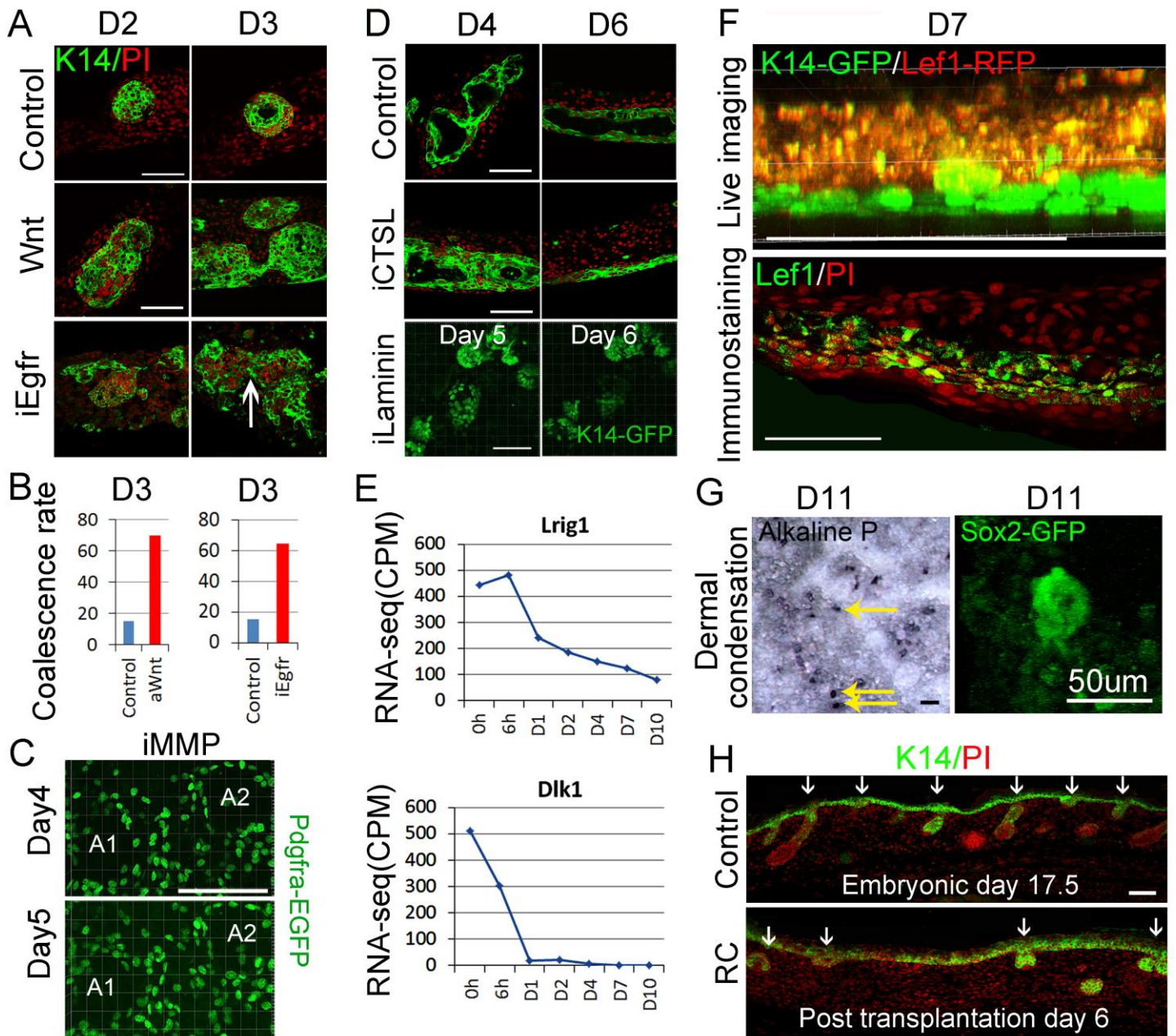


Fig. S7. Molecular mechanisms of the self-organization process from polarized aggregates to planar skin. (A-B) Immunostaining for K14 and related statistical analysis show coalescence of epidermal aggregates is accelerated at day 3 after the cultures are treated with Wnt agonist or small molecules that inhibit Egfr. (C) Live-imaging analysis of cellular behaviors of Pdgfra-EGFP+ cells reveals coalescence of epidermal aggregates is blocked after the culture is treated by small molecules that inhibit MMPs. (D) Immunostaining for K14 shows coalescence of epidermal aggregates at day 4 and planar skin formation at day 6. (E) RNA-seq reveals both Lrig1 and Dlk1 which represent papillary and reticular dermal cells, respectively, are decreased during culture. Lrig1 disappears at day 1 but Dlk1 is maintained at a certain level until day 10. CPM, counts per million. (F) Upper panel: 3D

rendering of cultured cells from K14-GFP/Lef1-RFP mouse line shows Lef1-positive cells are adjacent to K14+ basal epidermal cells at day 7. Lower panel: Immunostaining shows 3 to 4 layers of Lef1-positive cells are located beside the epidermal plane. (G) Alkaline phosphatase staining and Sox2-GFP positive cells show dermal condensates form at day 11. (H) Compared to the skin which produces organized hair germs in spacing at embryonic day 17.5, the reconstituted skin forms hair germs in a random distance. RC= reconstituted skin; Scale bars=100um, 50um.

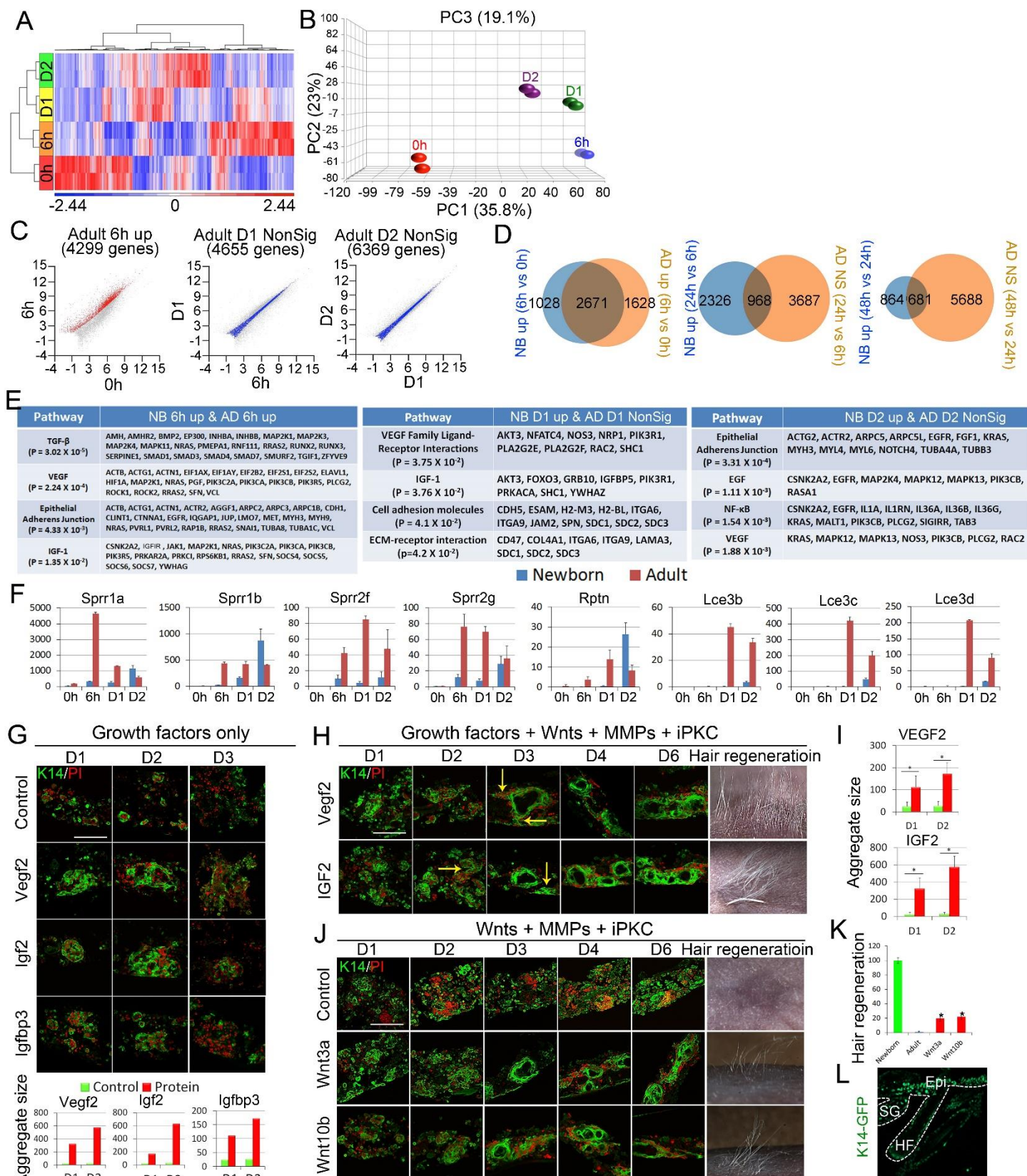














Fig. S8. Adult mice cells can be rescued to form hairs. (A) Hierarchical clustering shows genes that are dynamically expressed at different time points. (B) Principal component analysis (PCA) shows replicates cluster together. (C) RNA-seq data show three different groups of molecules are increased








at 6h or not significantly changed (NonSig) at day 1 and day 2. (D) Venn diagrams show the number of genes that are differentially expressed between newborn and adult mice cells at different time points. (E) Functional annotations show pathways and genes that are dynamically expressed at different time points. (F) EDC genes (e.g. Lce3b and Lce3c) are not highly expressed until day 7 in newborn cultures, but begin to increase at 6h in adult cultures. (G) Immunostaining for K14 shows aggregates can grow larger after the adult cell assays are treated with Vegf2, IGF2 and IGFBP3 recombinant proteins, but differentiate at day 3. (H-I) The self-organization process in newborn cell culture can take place in adult cell assays after they are sequentially treated with PKC inhibitors, recombinant proteins (VEGF2 and IGF2), Wnt recombinant proteins and MMPs. (J) Adult cell assays treated with Wnt3a or Wnt10b recombinant proteins from 0 h to day 4 can grow larger in size. (K) More hairs are regenerated when Wnts-treated adult cells are transplanted onto the back of nude mice. (L) K14-GFP shows the regenerated hair follicles are derived from donor cells. Epi, epidermis. SG, sebaceous gland. HF, hair follicle. Scale bars=100um. n=9. Data are reported as average \pm SD. *P < 0.05.

Supplemental Table S1 Gene ontology and pathways


























Newborn mouse cells 6h vs 0h

Term	RT	Genes	Count	%	P-Value
Cytokine-cytokine receptor interaction	RT		68	2.5	1.20E-09
Proteasome	RT		21	0.8	6.10E-07
Apoptosis	RT		29	1.1	3.40E-06
Jak-STAT signaling pathway	RT		41	1.5	9.20E-06
p53 signaling pathway	RT		22	0.8	1.40E-04
Cell adhesion	RT		23	0.8	2.20E-04
Spliceosome	RT		32	1.2	2.60E-04
NOD-like receptor signaling pathway	RT		20	0.7	2.60E-04
Insulin signaling pathway	RT		25	0.9	9.40E-03
Tight junction	RT		29	1.1	9.20E-03
TGF-beta signaling pathway	RT		25	0.9	2.60E-04
Regulation of actin cytoskeleton	RT		43	1.6	6.20E-03

Newborn mouse cells D1 vs 6h

Term	RT	Genes	Count	%	P-Value
cell adhesion	RT		101	3.7	4.30E-11
calcium	RT		165	6.1	5.20E-11
ECM-receptor interaction	RT		35	1.3	2.70E-10
zymogen	RT		61	2.2	1.40E-09
collagen	RT		34	1.3	5.60E-09
Valine, leucine and isoleucine degradation	RT		23	0.8	1.30E-08
Focal adhesion	RT		52	1.9	1.2E-06

Newborn mouse cells D2 vs D1

Term	RT	Genes	Count	%	P-Value
ribosome	RT		47	3.3	1.10E-12
extracellular region	RT		190	13.5	3.60E-09
proton-transporting V-type ATPase complex	RT		10	0.7	2.00E-06
cornified envelope	RT		10	0.7	3.60E-06
extracellular region part	RT		94	6.7	4.20E-06
proton-transporting two-sector ATPase complex	RT		14	1	7.90E-06
extracellular matrix	RT		43	3.1	1.40E-04
proteinaceous extracellular matrix	RT		41	2.9	2.50E-04
cytosolic ribosome	RT		7	0.5	1.60E-03
apical part of cell	RT		21	1.5	3.10E-03
extracellular space	RT		56	4	4.80E-03
myosin complex	RT		12	0.9	5.50E-03
cell-cell junction	RT		24	1.7	5.70E-03
apical plasma membrane	RT		16	1.1	7.30E-03
apical junction complex	RT		16	1.1	8.70E-03
apicolateral plasma membrane	RT		16	1.1	1.00E-02
organelle membrane	RT		79	5.6	1.50E-02
extracellular matrix part	RT		14	1	2.10E-02
endoplasmic reticulum	RT		80	5.7	2.40E-02
melanosome	RT		13	0.9	2.60E-02
pigment granule	RT		13	0.9	2.60E-02
occluding junction	RT		12	0.9	2.70E-02
tight junction	RT		12	0.9	2.70E-02
VEGF signaling pathway	RT		11	0.8	0.075
Gap junction	RT		12	0.9	7.50E-02

Newborn mouse cells D4 vs D2

Term	RT	Genes	Count	%	P-Value
Lysosome	RT		34	2.9	2.80E-13
Other glycan degradation	RT		8	0.7	3.20E-05
Glycosaminoglycan degradation	RT		8	0.7	4.60E-04
Focal adhesion	RT		26	2.2	9.90E-04
Leukocyte transendothelial migration	RT		18	1.5	1.70E-03
Regulation of actin cytoskeleton	RT		27	2.3	1.70E-03
Hypertrophic cardiomyopathy (HCM)	RT		14	1.2	2.80E-03
Adherens junction	RT		12	1	9.60E-03
Cell adhesion molecules (CAMs)	RT		19	1.6	1.10E-02
Glioma	RT		10	0.8	2.20E-02
Chronic myeloid leukemia	RT		11	0.9	2.50E-02
NOD-like receptor signaling pathway	RT		9	0.8	4.70E-02
Aldosterone-regulated sodium reabsorption	RT		7	0.6	5.30E-02
Non-small cell lung cancer	RT		8	0.7	5.90E-02
Pathways in cancer	RT		29	2.5	7.20E-02
Cytokine-cytokine receptor interaction	RT		23	1.9	7.50E-02
Dilated cardiomyopathy	RT		11	0.9	7.50E-02
ECM-receptor interaction	RT		10	0.8	0.089
extracellular matrix	RT		32	2.7	1.20E-02
proteinaceous extracellular matrix	RT		31	2.6	0.012

Newborn mouse cells D7 vs D4

Term	RT	Genes	Count	%	P-Value
Lysosome	RT		40	1.5	6.60E-07
Adherens junction	RT		24	0.9	4.90E-04
Pentose phosphate pathway	RT		12	0.4	7.00E-04
Arginine and proline metabolism	RT		18	0.7	1.30E-03
MAPK signaling pathway	RT		59	2.2	1.30E-03
ABC transporters	RT		16	0.6	1.60E-03
Toll-like receptor signaling pathway	RT		27	1	2.20E-03
Glutathione metabolism	RT		17	0.6	2.80E-03
ErbB signaling pathway	RT		24	0.9	3.60E-03
Glycolysis / Gluconeogenesis	RT		20	0.7	4.00E-03
Aminoacyl-tRNA biosynthesis	RT		14	0.5	6.50E-03
Porphyryn and chlorophyll metabolism	RT		11	0.4	0.0093
Oxidative Stress Induced Gene Expression Via Nrf2	RT		9	0.3	1.30E-02
Keratinocyte Differentiation	RT		14	0.5	0.017

CD40L Signaling Pathway	RT		7	0.3	2.00E-02
NF-kB Signaling Pathway	RT		9	0.3	2.60E-02

Newborn mouse cells D10vs D7

Term	RT	Genes	Count	%	P-Value
cornified envelope	RT		16	0.6	2.20E-10
endomembrane system	RT		126	4.7	3.50E-10
Golgi apparatus	RT		149	5.5	2.10E-09
nuclear envelope	RT		46	1.7	2.50E-07
extrinsic to membrane	RT		103	3.8	9.10E-07
endosome	RT		63	2.3	1.70E-06
internal side of plasma membrane	RT		68	2.5	4.80E-06
plasma membrane	RT		470	17.4	5.90E-06
desmosome	RT		12	0.4	1.50E-05
nuclear pore	RT		22	0.8	1.70E-05
plasma membrane part	RT		277	10.2	3.40E-05
Wnt signaling pathway	RT		40	1.5	1.20E-04
Neurotrophin signaling pathway	RT		36	1.3	1.50E-04
Ubiquitin mediated proteolysis	RT		37	1.4	1.70E-04
Chronic myeloid leukemia	RT		24	0.9	3.30E-04
Glioma	RT		21	0.8	5.00E-04
ECM-receptor interaction	RT		24	0.9	1.30E-03
Lysosome	RT		31	1.1	1.40E-03

Table S2. Antibodies used in this study.

Antibody	Isotype	Company	Cat #
β -catenin	Rabbit	Sigma	C2206
Collagen I	Rabbit	Abcam	ab34710
Collagen IV	Rabbit	Abcam	ab19808
DSC2/3	Mouse	Santa Cruz	sc-53485
DSG3	Mouse	MBL	D218-3
E-cadherin	Rabbit	Abcam	ab15148
Involucrin	Rabbit	Covance	PRB-142C

K10	Mouse	Santa Cruz	sc-52318
K14	Mouse	Santa Cruz	sc-53072
NCAM	Rabbit	Chuong CM	N/A
P63	Rabbit	Santa Cruz	sc-8343
P-cadherin	Goat	Santa Cruz	sc-1501
PCNA	Mouse	Santa Cruz	sc-56
PDGFra	Rat	eBioscience	14-1401-82
Vimentin	Rabbit	Cell signaling	5741S

Table S3. Primers used in this study.

Gene	Primer (5' to 3')
Col3a1-AS	gTAATACGACTCACTATAGGGatccatcttgccatcttcg
Col3a1-S	atggacgcaatggagaaaag
Col6a1-AS	CTAATACGACTCACTATAGGGgggcctggtagtttggtaca
Col6a1-S	tcgaaaccaccaaggctcttc
Ctsl-AS	CTAATACGACTCACTATAGGGccttgcgtccatagcaacaga
Ctsl-S	atgaggaattcaggcaggtg
Dcn-AS	CTAATACGACTCACTATAGGGaagtcattttgcccaactgc
Dcn-S	aaaatgcccagaactctcca
Igfbp3-AS	CTAATACGACTCACTATAGGGgtacgtcgtctttccccttg
Igfbp3-S	caggcagcctaagcacctac
Klk6-AS	CTAATACGACTCACTATAGGGcggtgtaaactcctggcttc
Klk6-S	ccgaatctgcaggtgatctt
Klk7-AS	CTAATACGACTCACTATAGGGccaccgttgtacttgcaga
Klk7-S	caagtacagctgggcagtga
Krt16-AS	CTAATACGACTCACTATAGGGgaaggccagctcttctctga

Krt16-S	acctcctctcgcttctcctc
Krt17-AS	CTAATACGACTCACTATAGGGtgccatcctgaacttctcc
Krt17-S	gaaccacgaggaggagatga
Lamc2-AS	CTAATACGACTCACTATAGGGgtcgttctcttggtccttg
Lamc2-S	atgcctctgggaactgtgac
Lce1d-AS	CTAATACGACTCACTATAGGGagtccccagactgttgcta
Lce1d-S	atgtcctgccagcaaagc
Lce1e-AS	CTAATACGACTCACTATAGGGcagcagcagtccccagac
Lce1e-S	ctgtcagcagagccagca
Mmp13-AS	gTAATACGACTCACTATAGGGtgggccattgaaaaagtag
Mmp13-S	gccatttcattgcttctgat
Mmp14-AS	CTAATACGACTCACTATAGGGcgtcaaacaccagtgctta
Mmp14-S	ttgatggtgaaggagggttc
Spr1a-AS	CTAATACGACTCACTATAGGGctgctggtatggtgatggag
Spr1a-S	atgagttcccaccagcagaa
Spr1b-AS	CTAATACGACTCACTATAGGGgctttgtcttctgttggcta
Spr1b-S	tgagttcacatcagcagaagc
Spr2f-AS	CTAATACGACTCACTATAGGGgcatttctgctggaatgagg
Spr2f-S	aagaacagcagtgcaagcaa
Tgfb1-AS	CTAATACGACTCACTATAGGGgagtctgccagctcatctcc
Tgfb1-S	tgataagaggggacggtttg
Vegfa-AS	CTAATACGACTCACTATAGGGgcattcacatctgctgtgct
Vegfa-S	ggtccagaaggagaggag

Table S4. Small molecule inhibitors and recombinant proteins used in this study.

Small molecule inhibitors

Catalog Number	Product Description	IC ₅₀
121767	AG 1024	IC ₅₀ = 7 mM for autophosphorylation of IGF-1R in intact cells
407248	IGF-1R Inhibitor II	IC ₅₀ = 12mM for inhibiting autophosphorylation of IGF-IR in MCF-7 cells IC ₅₀ <1 μM for IGF-R1
230751	Chromceptin IGF2 inhibitor	Blocks insulin-induced adipogenesis
121790	AGL 2043	IC ₅₀ = 800 nM for PDGFR in 3T3 cells IC ₅₀ = 90 nM against purified PDGFb-receptor
375670	Herbimycin A, Streptomyces sp.	IC ₅₀ = 8 μg/ml for PDGF-induced phospholipase D activation
521232	PDGF Receptor Tyrosine Kinase Inhibitor III	IC ₅₀ = 0.05 μM for α-PDGFR IC ₅₀ = 0.08 μM for β-PDGFR
440202	LY 294002	IC ₅₀ = 1.4 mM for phosphatidylinositol 3-kinase
676480	VEGF Receptor 2 Kinase Inhibitor I	
676481	VEGF Receptor Tyrosine Kinase Inhibitor II	IC ₅₀ = 20 nM, 180 nM and 240 nM for KDR, Flt-1 and c-Kit, respectively.
676483	VEGFR Tyrosine Kinase Inhibitor IV	IC ₅₀ = 50 nM, 6.5 nM, and 15 nM for VEGFR-1, VEGFR-2, VEGFR-3, respectively.
676487	VEGF Receptor 2 Kinase Inhibitor III	IC ₅₀ = 1.04 μM and 20 μM for VEGF-R (KDR/Flk-1) and PDGF-R tyrosine kinases in NIH 3T3 cells overexpressing Flk-1 IC ₅₀ = 50 nM, 5.3 μM and 30.5 μM for VEGF, bFGF, or ECGS, respectively. IC ₅₀ = 0.1 μM for ITD and FLT3 autophosphorylation
100066	NF-κB Activation Inhibitor V, 5HPP-33	Blocks IL-1-induced NF-κB translocation.

512732	Parthenolide, Tanacetum parthenium	NF- κ B Activation Inhibitor; inhibits MAPK
03-34-0051	Calpeptin	Calpain inhibitor
218713	Keratinocyte Differentiation Inducer	CKII inhibitor; keratinocyte differentiation inducer
616451	TGF- β RI Kinase Inhibitor	IC ₅₀ = 51 nM for TGF- β Receptor I kinase. IC ₅₀ = 89 nM for TGF- β -dependent cellular growth in NIH 3T3 mouse fibroblasts.
616453	TGF- β RI Inhibitor III	IC ₅₀ = 129 nM for activin receptor-like kinase 4. IC ₅₀ = 47 nM for activin receptor-like kinase 5. IC ₅₀ = 10.6 μ M for p38 MAPK α .
681665	Wnt Agonist	Selective activator of Wnt signaling
203696	BPIQ-I	IC ₅₀ = 0.025 nM for EGFR
324674	EGFR Inhibitor	IC ₅₀ = 21 nM, 63 nM, and 4 nM for EGFRwt, EGFR ^{L858R} and EGFR ^{L861Q} , respectively
513040	PD 174265 EGFR inhibitor	IC ₅₀ = 0.0450 μ M for EGFR
658390	AG 9	IC ₅₀ >1250 μ M for EGFR kinase
658552	AG 1478	IC ₅₀ = 3 nM for EGFR kinase.
688000	ROCK Inhibitor, Y- 27632	K _i = 140 nM for p160Rock (ROCK-I)
527450	PKR Inhibitor	IC ₅₀ = 210 nM for RNA-induced PKR autophosphorylation. IC ₅₀ = 100 nM rescue PKR-dependent translation block.
371806	GTP-14564	IC ₅₀ = 0.3 μ M for c-fms, c-kit, wt-FLT3 and ITD- FLT3 ¹ IC ₅₀ = 1.0 μ M for PDGFR β
420129	JNK Inhibitor V	IC ₅₀ = 150 nM for hJNK1 IC ₅₀ = 220 nM for hJNK2 IC ₅₀ = 70 nM for hJNK3

420135	JNK Inhibitor VIII	K _i = 2nM for JNK1 K _i = 4 nM for JNK2 K _i = 52 nM for JNK3
203297	Bisindolylmaleimide IV	IC ₅₀ = 87 nM for PKC
203290	Bisindolylmaleimide I	10nM
220285	Chelerythrine Chloride	660nM
SIGMA PZ0198	Prinomastat MMP inhibitor	50uM
APExBIO A4442	Way 170523 (MMP13 inhibitor)	100uM
Phoenix Pharmaceuticals, 038-08	Laminin binding inhibitor	10uM

Recombinant proteins

Catalog number	Protein	Concentration
MBS634420	IGFBP3	0.5ug/ml
R&D 792MG050	IGF2	10ng/ml
R&D 918MP010	MMP14	10ng/ml
MBS695709	Vegf2	25ng/ml
R&D 7196-WN-010	Wnt3a	10ng/ml
R&D 5036-WN-010	Wnt10b	10ng/ml